

¹ TraitHorizon: Scalable Exploration of Large Image-Feature Paired Datasets

³ **Jackson Jacobs**  ^{1*}, **Fan Fan**  ^{1*}, **Laura Barisoni**  ^{2,3}, and **Andrew Janowczyk**  ^{1,4,5¶}

⁵ 1 Department of Biomedical Engineering, Emory University and Georgia Institute of Technology, Atlanta, Georgia, USA 2 Department of Pathology, Division of AI and Computational Pathology, Duke University, Durham, North Carolina, USA 3 Department of Medicine, Division of Nephrology, Duke University, Durham, North Carolina, USA 4 Division of Precision Oncology, Department of Oncology, University Hospital of Geneva, Geneva, Switzerland 5 Division of Clinical Pathology, Department of Diagnostics, University Hospital of Geneva, Geneva, Switzerland ¶ Corresponding author * These authors contributed equally.

DOI: [10.xxxxxx/draft](https://doi.org/10.xxxxxx/draft)

Software

- [Review](#) 
- [Repository](#) 
- [Archive](#) 

Editor: 

Submitted: 01 December 2025

Published: unpublished

License

Authors of papers retain copyright and release the work under a Creative Commons Attribution 4.0 International License ([CC BY 4.0](#))

¹² 1. Summary

¹³ Collections of Objects of Interest (OOIs)—such as cells, tubules, or tissue patches—paired with high-dimensional, computationally derived feature vectors (e.g., morphology, texture, or deep-learned embeddings) are increasingly being generated in image-based biomedical research. These OOI-feature datasets are routinely explored to detect outliers for quality control, uncover patterns, and generate biological insights. However, as these datasets grow in size and complexity, researchers face several bottlenecks: repeated manual creation of static visualizations for each subpopulation, difficulties in efficiently plotting large numbers of high-dimensional feature vectors, and limited tooling for tracing individual feature values back to their source objects. To address these challenges, we developed TraitHorizon, a browser-based visualization platform for interactive exploration of large OOI–feature pair datasets. TraitHorizon integrates three synchronized visualization components: (a) a parallel coordinates plot for feature-vector-level exploration, (b) dynamic violin plots for per-feature distribution analysis, and (c) a tabular data grid linking each feature vector to its corresponding object. Its interactive interface enables real-time, scalable visualization of datasets containing hundreds of thousands of OOI-feature pairs. We demonstrate TraitHorizon’s utility through a case study involving quality control of a digital pathology dataset comprising 260,201 segmented tubules in kidney biopsies, each characterized by 99 features, illustrating how the platform facilitates rapid, interpretable, and reproducible data interrogation.

³¹ TraitHorizon is publicly available for use and modification at <https://traithorizon.com/>.

³² 2. Statement of Need

³³ Research in image-based fields (e.g., computational pathology) often aims to discover trends in Objects of Interest (OOIs), associated with diagnosis, prognosis, and therapy response. ³⁴ Objects can consist of individual items (e.g., cells), higher-order structures (e.g., tubules or infiltration patterns), or even small image patches. From these OOIs, sets of numerical features ³⁵ termed feature vectors are often extracted to encode their attributes. Features can range from ³⁶ simple (e.g., area, stain intensity, texture) to more complex, hand-crafted (e.g., aspect ratio of ³⁷ peritubular capillaries ([Yijiang Chen et al., 2025](#))), or even deep learning-derived descriptors ³⁸ ([Ambekar et al., 2025](#); [Y. Chen et al., 2023](#); [Yijiang Chen et al., 2025](#); [Echle et al., 2021](#); ³⁹ [Fan Fan et al., 2025](#)). These features can then be examined to assess their associations with ⁴⁰

42 object phenotypes—such as biological signals (e.g., disease state) or image quality factors
43 (e.g., blurriness)—or how they positively/negatively correlate with one another.

44 Such analysis often involve generating static, non-interactive, visualizations, such as a parallel
45 coordinates plots ([Heinrich & Weiskopf, 2013](#)) or scatter plots with UMAP ([McInnes et al.,](#)
46 [2020](#)) or t-SNE ([Maaten & Hinton, 2008](#)). Aided by first-order summary statistics (e.g., mean,
47 standard deviation), these visualizations are inspected to uncover structure and outliers within
48 the feature distribution. Multiple data-driven subpopulations often emerge from this initial
49 exploration, prompting repeated generation of visualizations and summary metrics for each
50 subpopulation. Quantitative and qualitative patterns uncovered within subpopulations can,
51 in turn, guide comparative analyses—for example, assessing how a given feature or pattern
52 differs between “diseased” and “normal” groups.

53 However, to date, this investigatory workflow remains time-intensive due to three main limiting
54 factors:

55 **1. Lack of connection between an object’s image, feature values, and cohort-level visualization.** Analysts often discover outliers or clusters within cohort-level visualizations,
56 prompting the need to trace them back to the associated images for visual inspection.
57 Static plots can at best display only a modest number of images, forcing analysts to
58 manually map plotted points to objects, incurring significant time costs. The ability to
59 instantly view the object associated with a plotted feature vector is essential for rapid
60 validation, interpretation, and insight generation.

61 **2. Exploring each subpopulation incurs high time cost.** Biomedical imaging datasets
62 often include heterogeneous subpopulations—such as tissue types, disease subtypes,
63 or experimental conditions—that warrant the generation of separate visualizations for
64 detailed inspection. Manually plotting each subpopulation becomes inefficient in repetitive
65 workflows, while programmatic (e.g., loop-based) plot generation requires subpopulations
66 of interest to be identified and well-defined *a priori*. Dynamic filtering and responsive
67 plots are necessary for users to iteratively explore subpopulations without incurring
68 substantial time costs from repeated plot generation and review. Furthermore, the
69 conditions/filters used to identify them should be easy to document, save, and reapply.

70 **3. Latency while rendering large datasets disrupts analysis.** OOI-feature datasets can easily
71 reach hundreds of thousands of data points. When subpopulations are not yet clearly
72 defined, a “global” view of the entire dataset is required before smaller subpopulations
73 can be explored. Browser-based tools not designed for plotting at this scale can suffer
74 from heavy memory utilization, latency, and even unresponsiveness/browser crashes while
75 rendering such data visualizations. A capable visualization tool must leverage rendering
76 techniques that remain efficient and within browser limitations as the number of objects
77 scales.

78 These limiting factors motivate the development of interactive data visualization tools that can
79 dynamically generate visualizations as the user explores their data. However, existing tools do
80 not fully address all three limiting factors simultaneously. TensorBoard Projector ([TensorFlow](#)
81 [Team, 2025](#)) and HoloViews ([Installation — HoloViews V1.21.0, n.d.](#)) support interactive
82 plotting of large multivariate datasets but do not provide for image viewing. Conversely,
83 DendroMap ([Bertucci et al., 2022](#)) facilitates qualitative exploration of large sets of images but
84 does not link back to their feature vectors. These tools also do not natively support dynamic
85 filtering by feature value. HistoQC ([Janowczyk et al., 2019](#)) provides image-linked plots and
86 metrics, but it is tailored specifically to quality control use cases in digital pathology and thus
87 does not support arbitrary user-defined features vectors or images.

88 To address these gaps, we introduce TraitHorizon, a browser-based application for interactive
89 exploration of images alongside their feature vectors. TraitHorizon (a) directly links plotted data
90 points to their source object images, enabling rapid validation and interpretation, (b) supports
91 dynamic, multi-dimensional filtering with support for saving and loading filter configurations,
92 and (c) efficiently renders hundreds of thousands of data points in-browser. By doing so,

94 TraitHorizon facilitates efficient exploratory analysis in object-based research workflows.

95 3. Implementation

96 TraitHorizon is a Flask-based application ([Pallets/Flask, n.d.](#)), making it ideal for collaborative
97 environments when hosted over a network. The front end is built with JavaScript, HTML5,
98 and CSS, and leverages visualization libraries such as SlickGrid ([SlickGrid Home, n.d.](#)), Parallel
99 Coordinates (parcoords ([Yun, 2025](#))), and D3.js ([D3 by Observable / The JavaScript Library
100 for Bespoke Data Visualization, n.d.](#)) to power its interactive dashboard. Its command-line
101 interface ingests a single directory of object image files (e.g., .png, .jpg, .svg, or any other
102 browser-supported format ("Image File Type and Format Guide - Media | MDN," 2025)) and
103 a tab-separated values (TSV) file, with each row containing an image file path followed by
104 a user-determined number of tab-separated feature columns. As such, any tool outputting
105 tabular data is compatible with TraitHorizon's simple input format (e.g., HistoQC ([Janowczyk
106 et al., 2019](#)) and CohortFinder ([Fan Fan et al., 2024](#))). TraitHorizon supports integer, float,
107 scientific notation, and categorical features. Clickable URLs are also supported by an optional
108 column titled "url".

109 TraitHorizon is designed to meet the demands of datasets containing hundreds of thousands of
110 objects. To minimize browser lag during plotting, five application features were implemented:

- 111 1. Non-blocking progressive rendering occurs in the parallel coordinates plot, completing in
112 seconds to minutes depending on dataset size. Importantly, the user interface remains
113 responsive during this rendering period, allowing users to continue interacting with the
114 parallel coordinates plot and other functional components without straining browser
115 responsiveness.
- 116 2. Parallel coordinate filter configurations and associated filtered object IDs can be exported
117 and imported in a lean JSON format, without requiring a re-render of the parallel
118 coordinates plot.
- 119 3. The data grid supports both pagination and alternatively "infinite scrolling". This web
120 design technique enables new content to be dynamically loaded, replacing old content
121 as the user scrolls down and creating the illusion of a never-ending page within a fixed
122 memory footprint.
- 123 4. Object images are loaded on-demand to limit browser memory, network utilization, and
124 CPU usage.
- 125 5. Violin plots are also computed on-demand when the user hovers over a parallel axis, avoiding
126 CPU usage associated with refreshing violin plots each time the parallel coordinates
127 plot is updated.

128 These design choices allow TraitHorizon to operate smoothly within the constraints of modern
129 web browsers and modest consumer-grade hardware, regardless of dataset size.

130 4. Use Case – Interactive Exploration of Tubular Pathomic 131 Features via TraitHorizon

132 To illustrate TraitHorizon's functionality, we provide the following detailed use case from
133 a recent digital pathology image-based biomarker study ([F. Fan et al., 2024; Fan Fan et
134 al., 2025](#)). In our use case, we focused on data exploration of 260,201 segmented tubules
135 ([Fogo et al., 2016](#)) and their associated features (for a total of 99 features per tubule) as
136 computed from 254 Periodic Acid-Schiff (PAS) stained kidney biopsies from the Nephrotic
137 Syndrome Study Network (NEPTUNE) ([Barisoni et al., 2013; Gadegbeku et al., 2013](#)) and
138 Cure Glomerulonephropathy (CureGN) ([CureGN Study Rationale, Design, and Methods, n.d.](#))
139 consortia. The goal was to support quality control and uncover tubular morphological patterns
140 along a pathway from normal to tubular atrophy ([Automated Computational Detection of](#)

¹⁴¹ *Interstitial Fibrosis, Tubular Atrophy, and Glomerulosclerosis / American Society of Nephrology,*
¹⁴² n.d.; Fogo et al., 2016).

¹⁴³ 4.1. Overview and Dataset Preparation

¹⁴⁴ Before running TraitHorizon, users must prepare a TSV file containing the following columns:

- ¹⁴⁵ 1. “**filename**” (**required**) – Specifies the base filename for each instance image, without
¹⁴⁶ the folder path (e.g., image1.png).
- ¹⁴⁷ 2. **Features (required)** – A tab separated row containing all features associated with each
¹⁴⁸ instance. Our dataset included 99 tubular pathomic features capturing morphological and
¹⁴⁹ topological characteristics of the basement membrane, epithelium, nuclei and lumen (Fan
¹⁵⁰ Fan et al., 2025). In our pre-TraitHorizon analysis, non-negative matrix factorization (F.
¹⁵¹ Fan et al., 2025; Lee & Seung, 2001) (rank = 14) followed by UMAP on these features
¹⁵² revealed 1,667 tubules forming outlier clusters. These were flagged in a separate “Needs
¹⁵³ QC” column.
- ¹⁵⁴ 3. “**url**” (**optional**) – Allows linking each object to external resources such as secondary
¹⁵⁵ visualizations, related analyses, or web-based viewers. In our use case, these URLs open
¹⁵⁶ the corresponding tubule in the HistomicsUI viewer (*DigitalSlideArchive/HistomicsUI*,
¹⁵⁷ 2025) within the Digital Slide Archive (DSA) (Gutman et al., 2017), which displays the
¹⁵⁸ tubule’s location within the original tissue slide for added histologic context.

¹⁵⁹ 4.2. Running TraitHorizon

¹⁶⁰ The folder containing all image files should be provided to TraitHorizon’s command-line
¹⁶¹ interface via the assets_path argument. All images must reside in this directory, which
¹⁶² TraitHorizon uses to locate and display them in the user interface. Similarly, the path to the
¹⁶³ TSV file should be specified using the tsv_path argument.

¹⁶⁴ After starting the TraitHorizon server, a local URL (e.g., <http://localhost:5000>) will appear in
¹⁶⁵ the terminal. Opening this URL in a web browser launches the TraitHorizon user interface
¹⁶⁶ (Figure 1), allowing users to interactively explore images and their associated features.

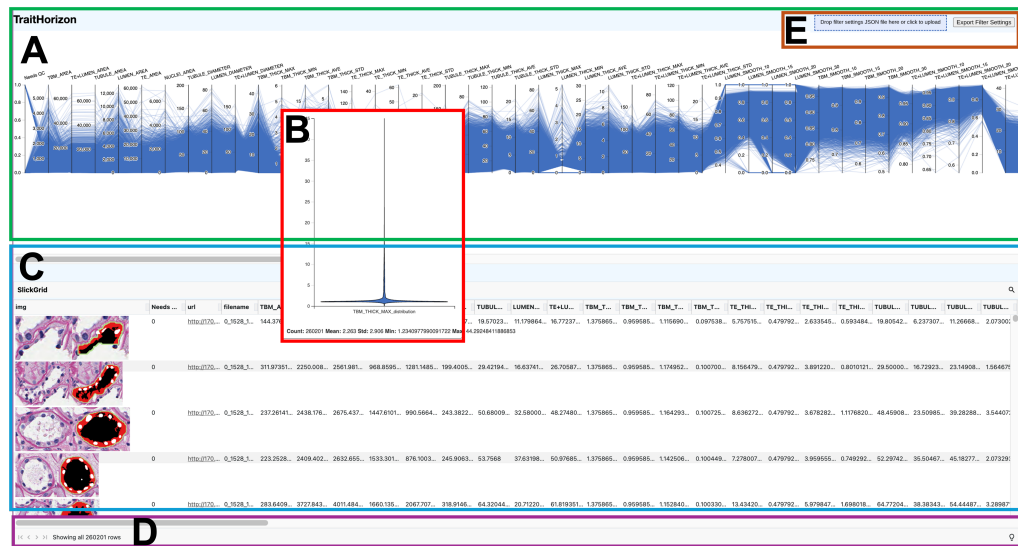


Figure 1: TraitHorizon web application interface. (A) The interactive parallel coordinates plot displays 99 pathomic features from 260,201 tubules, wherein each blue line represents one tubule feature vector. (B) A violin plot shows the value distribution of a selected feature when hovered over. (C) The data grid presents each segmented tubular image, with the original PAS-stained tubule on the left and the segmentation overlay on the right (green: tubular basement membrane; white: tubular nuclei; black: tubular lumen; red: tubular epithelium). Associated feature data loaded from the TSV (e.g., filename and corresponding feature values) are also displayed. (D) The bottom status bar shows the number of instances currently visible. (E) The drop zone and export button allow users to save filter configurations and filtered row IDs. TraitHorizon allows users to customize which columns are included or excluded in the parallel coordinates plot. Here, the URL and filename columns were excluded from the parallel coordinates plot but are shown in the data grid.

4.3. Initial Exploration with Parallel Coordinates Plots and Data Grid

Initial exploration began with the parallel coordinates plot, which provided a global view of feature distributions across hundreds of thousands of tubules (Figure 1-A). When hovering over a feature axis, a violin plot is displayed (Figure 1-B), enabling distribution visualization and noting of properties such as skewness and normality. Here, when hovering over the feature TBM_THICK_MAX (maximum tubular basement membrane thickness), the violin plot revealed a strongly skewed distribution. This suggested the presence of tubules with extremal values, which required closer examination in the data grid (Figure 1-C) for qualitative assessment. Together, these visualizations help users quickly identify whether features are broadly consistent, contain outliers, or show irregular patterns that may reflect artifacts or biologically distinct characteristics.

4.4. Filtering Based on Feature(s)

TraitHorizon's interactive filtering feature allows users to isolate and inspect data subpopulation based on feature values. For example, we filtered tubules with high TBM_THICK_MAX values (maximum tubular basement membrane thickness) by dragging a brush (Yun, 2025) along the corresponding axis in the parallel coordinate plot (Figure 2 – green box). The filtering action highlighted the relevant instances (tubules) in red and displayed their rows in the data grid, where we observed that these tubules consistently showed thickened basement membranes (large green segments), a hallmark of atrophic tubules.

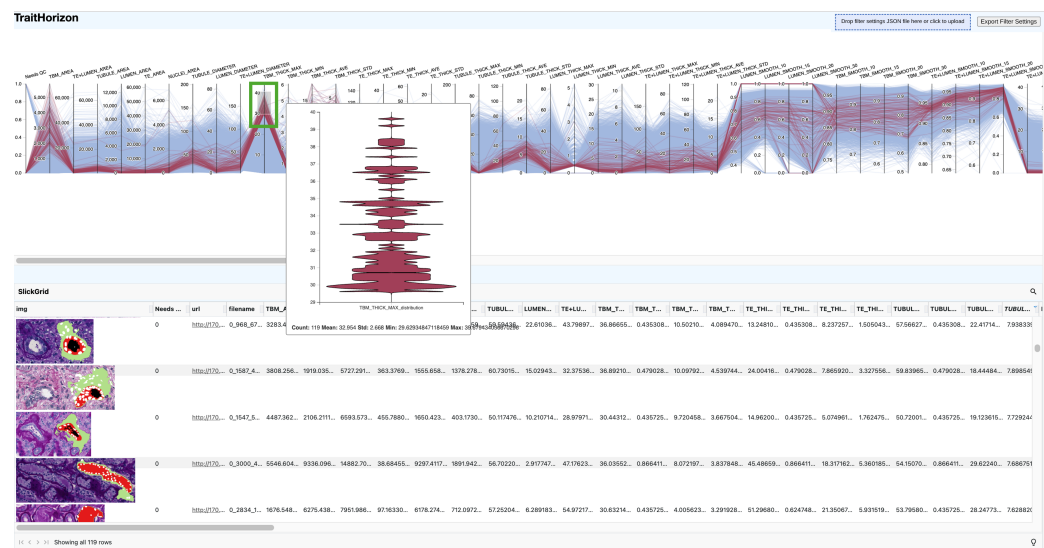


Figure 2: Interactive filtering with only one feature. TraitHorizon allows users to interactively filter instances based on any feature shown in the parallel coordinates plot. In this example, we hovered over the axis for the feature `TBM_THICK_MAX` (maximum basement membrane thickness) and dragged a brush to isolate tubules with values in the range from 30 to 40. In the parallel coordinate plot, 119 instances were dynamically highlighted in red after filtering (with this number indicated in the status bar), while all other ones remained visible but are greyed out. This color contrast makes it easier to visually compare the selected subset with the rest of the dataset across all other features. As shown here, the selected tubules were associated with visibly thickened basement membranes (enlarged green segments). Such interactive visualization enables users to explore and validate morphological patterns interactively. When hovering over a feature axis, a violin plot is generated for the selected subset (in red), providing an overview of feature-value distributions. In the data grid, only the filtered instances are shown.

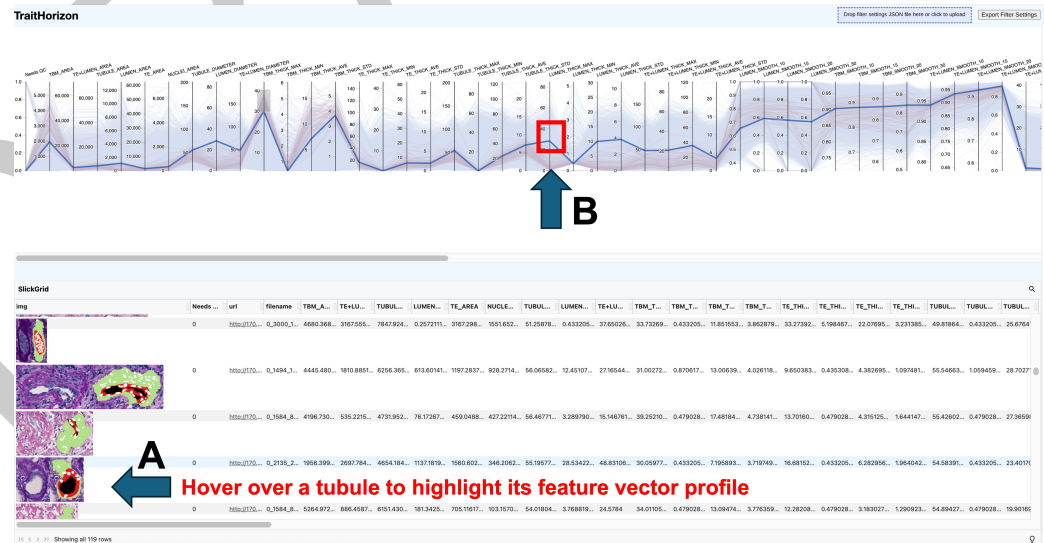


Figure 3: TraitHorizon enables the identification of multi-feature expression patterns. To inspect a specific instance, users can first (A) hover over the instance in the data grid, which highlights the corresponding row in both the parallel coordinates plot and the data grid in blue. By visually examining its feature vector, users can identify features of interest. In this example, the selected tubule showed high expression of `TBM_THICK_MAX`, and (B) moderate expression of `LUMEN_THICK_MAX` (maximum thickness of the tubular lumen).

186 TraitHorizon's data grid also displays images alongside their respective quantitative features,
 187 allowing users to explore individual instances in greater detail without switching contexts to
 188 perform image lookups. Using the data grid we visually examined the subset of tubules with
 189 high TBM_THICK_MAX values and found an unexpected phenotype characterized by enlarged
 190 lumina. When hovering over these rows in the data grid, the corresponding feature vectors
 191 were highlighted in blue within the parallel coordinates plot ([Figure 3-A](#)). Comparing the
 192 qualitative images with corresponding feature vectors suggested the existence of a small
 193 subpopulation of tubules exhibiting both thickened TBM and lumen dilation (moderately
 194 elevated values of LUMEN_THICK_MAX, the maximum lumen thickness; [Figure 3-B](#)). To further
 195 study this subpopulation, we applied an additional brush on LUMEN_THICK_MAX in the parallel
 196 coordinates plot ([Figure 4-2](#)). Subsequent review with study pathologists indicated that
 197 these tubules represent a composite morphological phenotype, combining basement membrane
 198 thickening with an enlarged lumen ([Fogo et al., 2016](#)).

199 In addition, TraitHorizon allows users to export and import filters for reproducibility and
 200 record-keeping. Specifically, clicking the "Export Filter Settings" button results in the filtered
 201 row IDs and corresponding filter values being saved as a JSON file ([Figure 4-3](#)). Dragging the
 202 JSON file into the drop zone ([Figure 4-4](#)) results in the brush being automatically restored
 203 and the corresponding subset of objects being reshown in the data grid.



Figure 4: Interactive joint filtering with multiple features. TraitHorizon supports joint filtering across multiple features to identify more complex patterns. In this example, we first (1) dragged a brush to isolate tubules with TBM_THICK_MAX values between 30 and 40, and then (2) applied a second brush on LUMEN_THICK_MAX, selecting values between approximately 15 and 25. This combined filtering enabled the identification of tubules showing both basement membrane thickening and enlarged lumen. Users can export filter configurations and filtered row IDs as a JSON file by clicking the (3) 'Export Filter Settings' button. For reproducibility, the exported JSON can later be reloaded by dragging it into the (4) drop zone, automatically restoring the filtering criteria.

204 Overall, the seamless integration of feature visualization, interactive filtering, and image
 205 review allows users to (1) rapidly assess whether unusual feature values reflect histopathological
 206 patterns or segmentation/technical artifacts, (2) uncover novel biological insights (e.g., complex
 207 disease phenotypes) that might be missed using univariate methods, ultimately supporting
 208 more informed QC and pattern exploratory analysis, (3) enhance reproducibility by enabling
 209 the storage, sharing, and restoration of filtering configurations for downstream analyses.

210 **4.5. External URL Integration for Contextual Visualization in HistomicsUI**

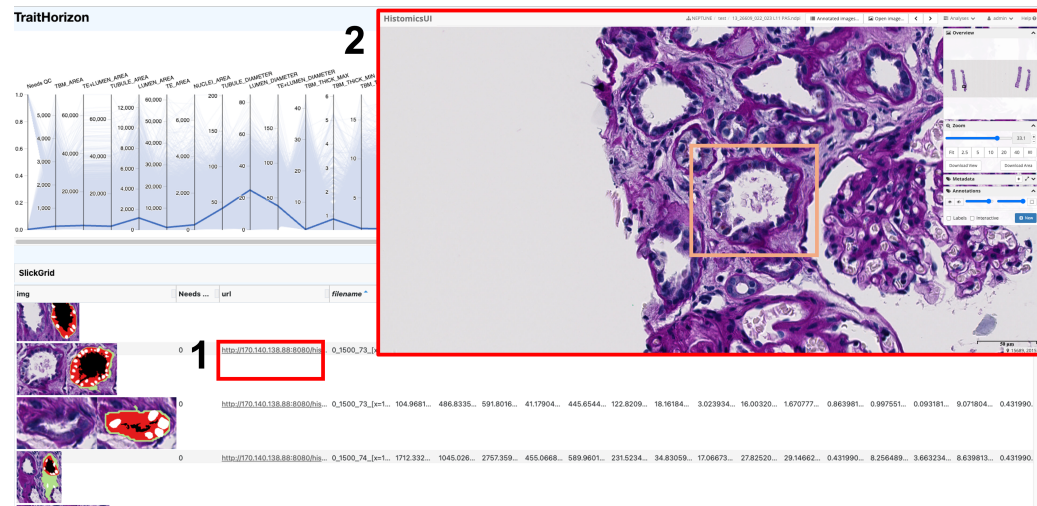


Figure 5: TraitHorizon supports integration with external viewers such as HistomicsUI through user-defined URL links. In this example, the link to the DSA has been pre-configured so that clicking the “url” cell of the row (1) opened an external browser window displaying the target tubule centered in the DSA’s HistomicsUI viewer (2). This functionality can also be used to connect objects to other external resources, such as clinical data, supplementary analyses, or metadata information.

211 TraitHorizon supports the integration of external URLs for each instance, enabling users to link
 212 directly to additional resources such as image viewers, annotation tools or clinical databases,
 213 depending on the needs of the workflow (Figure 5). In our implementation, this feature
 214 was used to connect TraitHorizon with DSA. Clicking the URL associated with each tubule
 215 (Figure 5-1) opened the corresponding region in the DSA’s viewer (named HistomicsUI) at
 216 the WSI level (Figure 5-2), with the tubule centered in view. This allowed pathologists to
 217 assess the broader tubule microenvironment—including adjacent tubules, interstitial areas, and
 218 glomeruli—rather than solely examining isolated objects. Notably, this feature is not limited
 219 to external image viewers but can be extended to any external resource to support different
 220 analytical workflows.

221 4.6. Searching by Exact Value

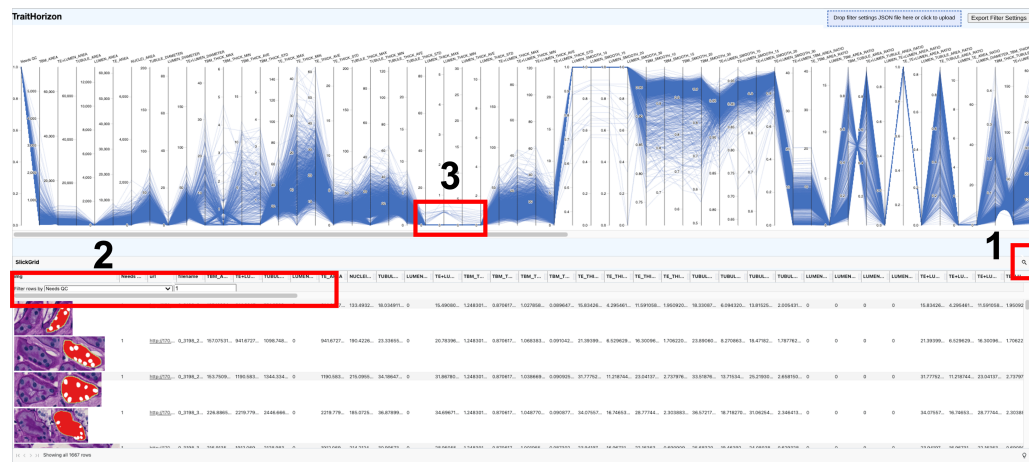


Figure 6: Flexible feature search. Using the user-defined “Needs QC” indicator (where ‘1’ marks tubules flagged for quality control), we (1) clicked the magnifier icon, and (2) manually entered the flag value to search the dataset. (3) The subset highlighted tubules lacking lumens, as evidenced by low values across lumen-related features such as LUMEN_THICK_AVE/MIN/MAX/STD (average, minimum, maximum, and standard deviation of tubular lumen thickness). This search functionality enables rapid identification of instances with specific feature values that need further review.

222 Beyond numerical range filtering, TraitHorizon also supports searching by specifying exact
 223 values for selected features. Users can (1) click the magnifier icon ([Figure 6-1](#)), (2) select the
 224 desired feature, and (3) input a specific category or value to search the dataset ([Figure 6-2](#)).
 225 Using this functionality, we searched for the “Needs QC” indicator to investigate tubules
 226 flagged for review. Visual inspection revealed that many flagged tubules lacked a visible lumen,
 227 and quantitative analyses (via the parallel coordinates plot) confirmed consistently low values
 228 for lumen-related features such as LUMEN_THICK_AVE (average lumen thickness, [Figure 6-3](#)).
 229 TraitHorizon thus enables rapid identification and efficient validation of instances with specific
 230 feature values—something that is often cumbersome in workflows using traditional/static tools.

231 Importantly, this search capability is not restricted to quality control indicators. It can be
 232 applied to any features in the dataset, enabling users to flexibly isolate and analyze subsets of
 233 interest based on labels, classifications, or other features. This is particularly useful for features
 234 containing numerous unique categories or identifiers—for example, identifying a specific tubule
 235 by its filename or retrieving all tubules originating from the same patient.

²³⁶ **4.7. Sorting Numerical Features**

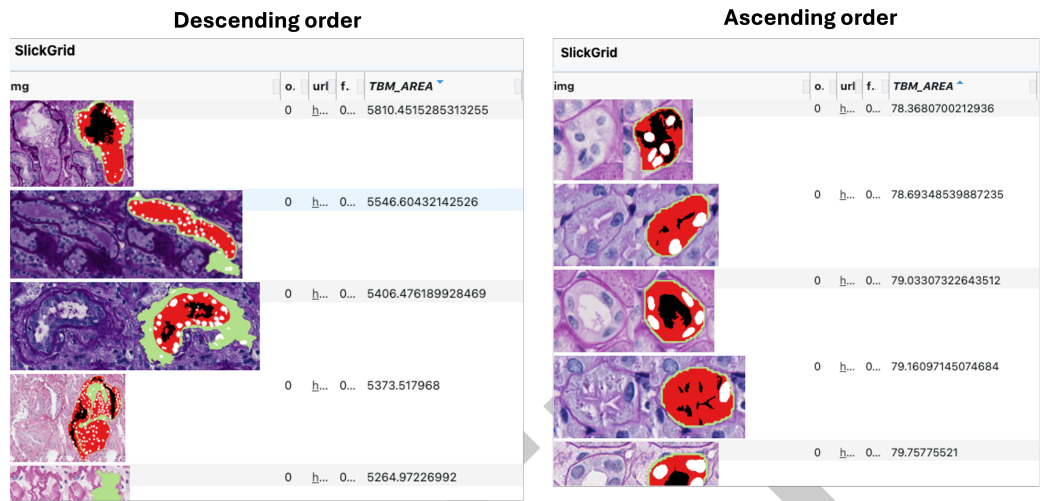


Figure 7: Sorting numerical features. TraitHorizon allows users to sort numerical features directly within the data grid by clicking on a column header. Features can be sorted in either descending (left) or ascending (right) order. In this example, the feature TBM_AREA (tubular basement membrane area) was sorted to facilitate comparison between tubules with large/thickened basement membranes and those with small/thin ones, helping users visually assess underlying morphological differences. In the descending view (left panel), the top-ranked tubules exhibited larger or thickened TBM regions (extensive green segments). Conversely, in ascending view (right panel), the top entries corresponded to tubules with smaller or thinner basement membranes. By sorting features interactively, users can identify qualitative gradients across ordered set of objects, revealing progressive feature changes within the dataset.

²³⁷ TraitHorizon also supports sorting of numerical features directly within the data grid by clicking
²³⁸ on a column header (Figure 7). In our workflow, we sorted tubules by TBM_AREA (tubular
²³⁹ basement membrane area) to explore morphological variation. Scrolling through the sorted grid
²⁴⁰ revealed a clear gradient in morphology—specifically, progressive thickening of the basement
²⁴¹ membrane—enabling intuitive observation of trends from normal to atrophic tubules.

²⁴² **5. Discussion and Conclusions**

²⁴³ TraitHorizon addresses a critical gap in image-based data analysis by enabling fast, interactive,
²⁴⁴ and image-linked exploration of high dimensional feature datasets. Traditional visualization
²⁴⁵ approaches often fail to couple image data with derived features and support interactive
²⁴⁶ plotting at scale. In contrast, TraitHorizon links each source image to its high dimensional
²⁴⁷ feature vector, supports real-time interactive filtering and sorting, and utilizes efficient rendering
²⁴⁸ strategies to scale to datasets with hundreds of thousands of images.

²⁴⁹ TraitHorizon's features empower researchers to discover meaningful patterns, perform quality
²⁵⁰ control, and generate insights for large object-feature datasets. Furthermore, TraitHorizon's
²⁵¹ support for arbitrary features, multiple feature types, and external URLs enable its broad use
²⁵² across multiple computational imaging fields.

²⁵³ TraitHorizon is available as a python package, and a Docker image is released for easy
²⁵⁴ installation (<https://traithorizon.com/>).

²⁵⁵ **6. Acknowledgements**

²⁵⁶ Research reported in this publication was supported by:

- 257 (1) the National Institutes of Health (NIH) under the following awards: R01LM013864 and
258 R01DK118431;
- 259 (2) The Nephrotic Syndrome Study Network (NEPTUNE) is part of the Rare Diseases Clinical
260 Research Network (RDCRN), which is funded by the NIH and led by the National Center
261 for Advancing Translational Sciences (NCATS) through its Division of Rare Diseases
262 Research Innovation (DRDRI). NEPTUNE is funded under grant number U54DK083912
263 as a collaboration between NCATS and the National Institute of Diabetes and Digestive
264 and Kidney Diseases (NIDDK). Additional funding and/or programmatic support is
265 provided by the University of Michigan, NephCure Kidney International, Alport Syndrome
266 Foundation, and the Halpin Foundation. RDCRN consortia are supported by the RDCRN
267 Data Management and Coordinating Center (DMCC), funded by NCATS and the National
268 Institute of Neurological Disorders and Stroke (NINDS) under U2CTR002818;
- 269 (3) Additional support was also provided by NephCure and the Henry E. Haller, Jr. Founda-
270 tion;
- 271 (4) Funding for the CureGN consortium is provided by U24DK100845, U01DK100846,
272 U01DK100876, U01DK100866, and U01DK100867 from the National Institute of Dia-
273 betes and Digestive and Kidney Diseases (NIDDK). Patient recruitment is supported
274 by NephCure. Dates of funding for first phase of CureGN was 9/16/2013-5/31/2019.
275 Dates of funding for the second phase of CureGN was 6/1/2019 - 5/31/2024.
- 276 NEPTUNE Collaborating Sites: Atrium Health Levine Children's Hospital, Charlotte, SC:
277 Susan Massengill, Layla Lo##; Cleveland Clinic, Cleveland, OH: Katherine Dell, John O'Toole,
278 John Sedor, Victoria Grange##; Children's Hospital, Denver, CO: Bradley Dixon, Nathan
279 Rogers##; Children's Hospital, Los Angeles, CA: Rachel Lestz, Natalie Esquivias##; Children's
280 Mercy Hospital, Kansas City, MO: Tarak Srivastava, Kelsey Markus##; Cohen Children's
281 Hospital, New Hyde Park, NY: Christine Sethna, Suzanne Vento##; Columbia University,
282 New York, NY: Pietro Canetta; Duke University Medical Center, Durham, NC: Opeyemi
283 Olabisi, Rasheed Gbadegesin, Maurice Smith##; Emory University, Atlanta, GA: Laurence
284 Greenbaum, Chia-shi Wang, Chris Fan##; The Lundquist Institute, Torrance, CA: Sharon Adler,
285 Janine LaPage##; John H Stroger Cook County Hospital, Chicago, IL: Amatur Amarah; Johns
286 Hopkins Medicine, Baltimore, MD: Meredith Atkinson, Ryan Hutson##; Mayo Clinic, Rochester,
287 MN: John Lieske, Marie Hogan, Fernando Fervenza; Medical University of South Carolina,
288 Charleston, SC: David Selewski, Cheryl Alston##; Montefiore Medical Center, Bronx, NY: Kim
289 Reidy, Michael Ross*, Frederick Kaskel**, Patricia Flynn##; New York University Medical
290 Center, New York, NY: Laura Malaga-Dieguez, Olga Zhdanova, Laura Jane Pehrson##, Melanie
291 Miranda##; The Ohio State University College of Medicine, Columbus, OH: Salem Almaani,
292 Laci Roberts##; Riley Children's Hospital of Indiana University, Indianapolis, IN: Myda Khalid,
293 Veronica Servin##; Stanford University, Stanford, CA: Richard Lafayette, Elizabeth Chen## ;
294 Temple University, Philadelphia, PA: Iris Lee; Texas Children's Hospital at Baylor College of
295 Medicine, Houston, TX: Shweta Shah, Thinh Phan## ; University Health Network Toronto:
296 Heather Reich, Michelle Hladunewich, Paul Ling##, Martin Romano##; University of California
297 at San Diego, San Diego, CA: Ambarish Athavale, Caitlin Carter, Kristin Zeeb##; University
298 of California at San Francisco, San Francisco, CA: Paul Brakeman, Daniel Schrader; University
299 of Colorado Anschutz Medical Campus, Aurora, CO: James Dylewski* Nathan Rogers##;
300 University of Kansas Medical Center, Kansas City, KS: Ellen McCarthy, Catherine Creed##;
301 University of Miami, Miami, FL: Alessia Fornoni, Miguel Bandes##; University of Michigan,
302 Ann Arbor, MI: Matthias Kretzler, Laura Mariani, Zubin Modi, Amanda Williams##, Roxy
303 Ni##; University of Minnesota, Minneapolis, MN: Patrick Nachman, Michelle Rheault, Ariel
304 Langenberger##, Brady Wallner##; University of North Carolina, Chapel Hill, NC: Vimal
305 Derebail, Keisha Gibson, Anne Froment##, Sharia Warren##; University of Pennsylvania,
306 Philadelphia, PA: Lawrence Holzman, Kevin Meyers, Krishna Kallem##, Arielle Swenson##;
307 University of Texas San Antonio, San Antonio, TX: Samin Sharma; University of Texas
308 Southwestern, Dallas, TX: Elizabeth Roehm, Kamalanathan Sambandam, Elizabeth Brown;
309 University of Washington, Seattle, WA: Ashley Jefferson, Sangeeta Hingorani, Katherine

310 **Tuttle§, Linda Manahan #, Emily Pao#, Kelli Kuykendall§; Wake Forest University Baptist**
311 **Health, Winston-Salem, NC: Jen Jar Lin; Washington University in St. Louis, St. Louis, MO:**
312 **Brian Stotter, Joseph Dumayas#**

313 Data Analysis and Coordinating Center: University of Michigan: Matthias Kretzler*, Brenda
314 Gillespie, **Laura Mariani**, Zubin Modi, Eloise Salmon, Howard Trachtman, **Tina Mainieri**,
315 Michael Arbit, Hailey Desmond, Sean Eddy, Damian Fermin, Wenjun Ju, Maria Larkina,
316 Chrysta Lienczewski, Rebecca Scherr, Jonathan Troost, Amanda Williams, Yan Zhai;;
317 **Cleveland Clinic: Crystal Gadegbeku**, John Sedor, Duke University: **Laura Barisoni**; Harvard
318 University: Matthew G Sampson; **Northwestern University: Abigail Smith**; University of
319 Pennsylvania: Lawrence Holzman, **Jarcy Zee**

320 NEPTUNE Digital Pathology Committee: Carmen Avila-Casado (University Health Network),
321 Serena Bagnasco (Johns Hopkins University), Lihong Bu (Mayo Clinic), Shelley Caltharp
322 (Emory University), Clarissa Cassol (Arkana), Dawit Demeke (University of Michigan), Brenda
323 Gillespie (University of Michigan), Jared Hassler (Temple University), Leal Herlitz (Cleveland
324 Clinic), Stephen Hewitt (National Cancer Institute), Jeff Hodgin (University of Michigan),
325 Danni Holanda (Arkana), Neeraja Kambham (Stanford University), Kevin Lemley, Laura
326 Mariani (University of Michigan), Nidia Messias (Washington University), Alexei Mikhalov
327 (Wake Forest), Vanessa Moreno (University of North Carolina), Behzad Najafian (University of
328 Washington), Matthew Palmer (University of Pennsylvania), Avi Rosenberg (Johns Hopkins
329 University), Virginie Royal (University of Montreal), Miroslav Sekulik (Columbia University),
330 Barry Stokes (Columbia University), David Thomas (Duke University), Ming Wu (University
331 of New York), Michifumi Yamashita (Cedar Sinai), Hong Yin (Emory University), Jarcy Zee
332 (University of Pennsylvania), Yiqin Zuo (University of Miami). Co-Chairs: **Laura Barisoni**
333 (Duke University), **Cynthia Nast** (Cedar Sinai)

334 The CureGN Consortium members listed below, from within the four Participating Clinical
335 Center networks and Data Coordinating Center, are acknowledged by the authors as
336 Collaborators.

337 **CureGN PCC Principal Investigators; *CureGN Site Principal Investigators; +CureGN
338 Pathologists, #CureGN Lead Coordinators.

339 CureGN Participating Clinical Centers (PCC) through Columbia University: Columbia University,
340 New York, NY, US: Gerald Appel, Revekka Babayev, Ibrahim Batal +, Andrew Bomback, **Pietro**
341 **Canetta, Brenda Chan, Vivette Denise D'Agati +, Samitri Dogra, Hilda Fernandez, Gabriele**
342 **Gaggero+**, Ali Gharavi, William Hines, , Krzysztof Kiryluk**, Satoru Kudose +, Fangming Lin,
343 Victoria Kolupaeva#, Maddalena Marasa, Glen Markowitz +, Mariela Navarro-Torres, Hila
344 Milo Rasouly, Sumit Mohan, Nicola Mongera, Jordan Nestor, Jai Radhakrishnan, Maya Rao,
345 Maya Sabatello, Simone Sanna-Cherchi, Dominick Santoriello+, Miroslav Sekulic +, , Michael
346 Barry Stokes+, Natalie Uy, Natalie Vena, Benjamin Wooden; University of Warsaw, Warszawa,
347 Poland: Bartosz Foroncewicz, Natalia Wiewiórska-Krata, Barbara Mosczuk, Krzysztof Mucha*,
348 Agnieszka Perkowska-Ptasińska, Elżbieta Ryszkowska; IRCCS Giannina Gaslini, Genoa, Italy:
349 Francesca Lugani, Valerio Vellone+

350 CureGN Participating Clinical Centers (PCC) through the Pediatric Nephrology Research
351 Consortium: Children's Hospital of New Orleans/ LSU Health, New Orleans, LA, USA:
352 Diego Aviles; **Children's Mercy Hospital, Kansas City, MO, USA: Tarak Srivastava, Alexander**
353 **Katz+**; Children's National Medical Center, Washington DC, USA: Sun-Young Ahn; **Cincinnati**
354 **Children's Hospital Cincinnati, OH, USA: Prasad Devarajan, Elif Erkan, Hillarey Stone**;
355 Connecticut Children's Medical Center, Hartford, CT, USA: Sherene Mason; **East Carolina**
356 **University Brody School of Medicine, Greenville, NC, USA: Liliana Gomez-Mendez**; Emory
357 University, Atlanta, GA, USA: Larry Greenbaum, Chia-shi Wang, Hong (Julie) Yin+ ;
358 **Helen DeVos Children's Hospital, Grand Rapids, MI, USA: Goebel Jens; Levine Children's**
359 **Hospital/Atrium Health, Charlotte, NC, USA: Donald Weaver; Lurie Children's Hospital,**
360 **Chicago IL, USA: Jill Krissberg, Jerome Lane; Medical College of Wisconsin, Milwaukee,**
361 **WI, USA: Cindy Pan, Ellen Cody; Nationwide Children's Hospital, Columbus, OH, USA:**

362 **Samantha Martinek-Bundt#**, Dawson Carmean#, Mary Dreher#, Mahmoud Kallash, John
 363 Mahan, Samantha Sharpe#, William Smoyer, Laura Biederman+; Oregon Health and Science
 364 University, Portland, OR, USA; Amira Al-Uzri, Sandra Iragorri ; Riley Children's Hospital,
 365 Indianapolis, IN, USA; Myda Khalid; Cardinal Glennon Children's Medical Center/ St. Louis
 366 University, St. Louis, MO, USA; Craig Belsha; Texas Children's Hospital, Houston, TX, USA;
 367 Elizabeth Onugha, Michael Braun, AC Gomez; Texas Tech Health Sciences Center, Amarillo,
 368 TX, USA; Tetyana Vaslyeva; Children's of Alabama, University of Alabama, Birmingham, AL,
 369 USA; Daniel Feig; University of Colorado Children's Hospital, Colorado, Aurora, CO, USA;
 370 Melisha Hannah; University of Kentucky, Lexington, KY, USA; Aftab Chishti; University of
 371 Louisville, Louisville, KY, USA; Jon Klein**; Holtz Medical Center, University of Miami, Miami,
 372 FL, USA; Chryso Katsoufis, Wacharee Seeherunvong*; University of Minnesota Children's
 373 Hospital, Minneapolis, MN, USA; Michelle Rheault**; University of New Mexico Health
 374 Sciences Center, Albuquerque, NM, USA; Craig Wong; University of Oklahoma Health Sciences
 375 Center, Oklahoma City, OK, USA; Qassim Abid; University of Virginia, Charlottesville, VA,
 376 USA; John Barcia, Agnes Swiatecka-Urban; University of Wisconsin, Madison, WI, USA;
 377 Sharon Bartosh; Washington University in St. Louis, St. Louis, MO, USA; Brian Stotter*,
 378 Joseph Gaut +

379 CureGN Participating Clinical Centers (PCC) through the University of North Carolina: Hôpital
 380 Maisonneuve-Rosemont, Montreal, Canada: Louis-Philippe Laurin, Virginie Royal+, Mathieu
 381 Latour+, Natlie (Natacha) Patey +; Medical University of South Carolina, Charleston, SC,
 382 USA; Anand Achanti, Milos Budisavljevic, Vishwajeeth Pasham+; Northwestern University,
 383 Chicago, IL, USA; Cybele Ghossein, Yonatan Peleg; Ohio State University, Columbus, OH,
 384 USA; Salem Almaani, Isabelle Ayoub, Samir Parikh, Brad Rovin, Anjali Satoskar+; University
 385 of Chicago, Chicago, IL, USA; Anthony Chang+ ; University of Alabama at Birmingham,
 386 Birmingham, AL, USA; Huma Fatima+, Jan Novak, Matthew Renfrow, Dana Rizk; University
 387 of North Carolina Kidney Center, Chapel Hill, NC, USA; Dhruti Chen, Vimal Derebail, Ronald
 388 Falk, Keisha Gibson, Dorey Glenn, Susan Hogan, Koyal Jain, J. Charles Jennette+, Vanessa
 389 Moreno+, Amy Mottl, Caroline Poulton#, Monica Reynolds, Manish Kanti Saha, Nicole E.
 390 Wyatt; Vanderbilt University, Nashville, TN, USA; Agnes Fogo+, Neil Sanghani; Virginia
 391 Commonwealth University, Richmond, VA, USA; Jason Kidd*, Selvaraj Muthusamy+

392 CureGN Participating Clinical Centers (PCC) through the University of Pennsylvania: Children's
 393 Hospital of Philadelphia, Philadelphia, PA, USA; Rebecca Scobell, Michelle Denburg, Amy
 394 Kogon, Kevin Meyers, Madhura Pradhan; Cleveland Clinic, Cleveland, OH, CA; Raed Bou
 395 Matar, John O'Toole, John Sedor; Cohen Children's Medical Center, New Hyde Park, NY,
 396 USA; Christine Sethna**, Suzanne Vento#; Johns Hopkins University, Baltimore, MD, USA:
 397 Mohamed Atta, Serena Bagnasco+, Alicia Neu, John Sperati; Lundquist Institute at Harbor-
 398 UCLA Medical Center, Torrance, CA, USA; Sharon Adler, Tiane Dai, Ram Dukkipati; Montefiore
 399 Medical Center, The Bronx, New York, NY, USA; Frederick Kaskel, Kaye Brathwaite, Kimberly
 400 Reidy; New York University, New York, NY, USA; Laura Malaga-Dieguez; Spokane Providence
 401 Medical Center, Spokane, WA, USA; Katherine Tuttle; Stanford University, Palo Alto, CA,
 402 USA; Richard Lafayette, Kamal Fahmeedah, Elizabeth Talley; Sunnybrook Health Sciences
 403 Centre, Toronto, Canada: Michelle Hladunewich; The Hospital for Sick Children, Toronto,
 404 Canada; Rulan Parekh; University Health Network, Toronto, Canada: Carmen Avila-Casado+,
 405 Daniel Cattran, Reich Heather, Meherzad Kutky ; University of Miami, Miami, FL, USA;
 406 Yelena Drexler, Alessia Fornoni; University of Michigan, Ann Arbor, MI, USA; Jeffrey Hodgin+,
 407 Andrea Oliverio*; University of Pennsylvania, Philadelphia, PA, USA; Jon Hogan, Lawrence
 408 Holzman**, Matthew Palmer +, Gaia Coppock; University of Pittsburgh School of Medicine,
 409 Pittsburgh, PA, USA; Michael Mortiz, Juhi Kumar; University of Washington, Seattle, WA,
 410 USA; Charles Alpers+, J. Ashley Jefferson; UT Southwestern, Dallas, TX, USA; Kamal
 411 Sambandam, Bethany Roehm*Data Coordinating Center (DCC): Cedar Sinai Medical Center,
 412 Los Angeles, CA, USA; Cynthia Nast+, Jean Hou+; Duke University, Durham, NC, USA;
 413 Laura Barisoni; Cleveland Clinic, Cleveland, OH, USA; Crystal Gadegbeku; Northwestern
 414 University, Chicago, IL, USA; Abigail Smith ; University of Michigan, Ann Arbor, MI, USA;
 415 Brenda Gillespie, Bruce Robinson, Matthias Kretzler, Zubin Modi, Laura Marianj**

416 Steering Committee Chair: Lisa M. Guay-Woodford, Children's Hospital of Pennsylvania,
417 Philadelphia, PA, USA

418 7. References

- 419 Ambekar, A., Roohian, M., Liu, Q., Wang, B., Fan, F., Cassol, C., Lafata, K., Holzman,
420 L., Mariani, L., Hodgin, J., Zee, J., Janowczyk, A., & Barisoni, L. (2025). *Glomerular
421 Segmentation, Classification, and Pathomic Feature-based Prediction of Clinical Outcomes
422 in Minimal Change Disease and Focal Segmental Glomerulosclerosis*. medRxiv. <https://doi.org/10.1101/2025.10.01.25336172>
- 424 *Automated Computational Detection of Interstitial Fibrosis, Tubular Atrophy, and Glomeru-
425 losclerosis / American Society of Nephrology*. (n.d.). Retrieved August 29, 2022, from
426 <https://jasn.asnjournals.org/content/32/4/837.abstract>
- 427 Barisoni, L., Nast, C. C., Jennette, J. C., & others. (2013). Digital pathology evaluation in
428 the multicenter Nephrotic Syndrome Study Network (NEPTUNE). *Clinical Journal of the
429 American Society of Nephrology (CJASN)*, 8(8), 1449–1459. <https://doi.org/10.2215/CJN.08370812>
- 431 Bertucci, D., Hamid, M. M., Anand, Y., Ruangrotsakun, A., Tabatabai, D., Perez, M., &
432 Kahng, M. (2022). *DendroMap: Visual Exploration of Large-Scale Image Datasets for
433 Machine Learning with Treemaps*. arXiv. <https://doi.org/10.48550/arXiv.2205.06935>
- 434 Chen, Yijiang, Wang, B., Demeke, D., Fan, F., Berthier, C., Mariani, L., Lafata, K., Holzman,
435 L., Hodgin, J., Janowczyk, A., Barisoni, L., & Madabhushi, A. (2025). Clinical relevance
436 of computational pathology analysis of interplay between kidney microvasculature and
437 interstitial microenvironment. *Clinical Journal of the American Society of Nephrology*,
438 20(2), 239–255. <https://doi.org/10.2215/CJN.0000000597>
- 439 Chen, Y., Zee, J., Janowczyk, A. R., Rubin, J., Toro, P., Lafata, K. J., Mariani, L. H.,
440 Holzman, L. B., Hodgin, J. B., Madabhushi, A., & Barisoni, L. (2023). Clinical relevance of
441 computationally derived attributes of peritubular capillaries from kidney biopsies. *Kidney360*,
442 4(5), 648–658. <https://doi.org/10.34067/KID.0000000000000116>
- 443 *CureGN Study Rationale, Design, and Methods: Establishing a Large Prospective Observational
444 Study of Glomerular Disease - PubMed*. (n.d.). Retrieved May 30, 2024, from <https://pubmed.ncbi.nlm.nih.gov/30420158/>
- 446 *D3 by Observable / The JavaScript library for bespoke data visualization*. (n.d.). Retrieved
447 July 9, 2025, from <https://d3js.org/>
- 448 *DigitalSlideArchive/HistomicsUI*. (2025). Digital Slide Archive. [https://github.com/DigitalSlideArchive/HistomicsUI](https://github.com/
449 DigitalSlideArchive/HistomicsUI)
- 450 Echle, A., Rindtorff, N. T., Brinker, T. J., Luedde, T., Pearson, A. T., & Kather, J. N. (2021).
451 Deep learning in cancer pathology: A new generation of clinical biomarkers. *Br J Cancer*,
452 124(4), 686–696. <https://doi.org/10.1038/s41416-020-01122-x>
- 453 Fan, F., Liu, Q., Zee, J., & others. (2024). Computationally derived characterization of tubular
454 changes in relation to the development of interstitial fibrosis: FR-PO933. *Journal of the
455 American Society of Nephrology*, 35(10S). <https://doi.org/10.1681/ASN.20248v5y8bw>
- 456 Fan, Fan, Liu, Q., Zee, J., Ozeki, T., Demeke, D., Yang, Y., Bitzer, M., O'Connor, C. L.,
457 Farris, A. B., Wang, B., Shah, M., Jacobs, J., Mariani, L., Lafata, K., Rubin, J., Chen, Y.,
458 Holzman, L., Hodgin, J. B., Madabhushi, A., ... Janowczyk, A. (2025). Clinical relevance of
459 computationally derived tubular features and their spatial relationships with the interstitial
460 microenvironment in minimal change disease/focal segmental glomerulosclerosis. *Kidney
461 International*, 0(0). <https://doi.org/10.1016/j.kint.2025.04.026>

- 462 Fan, Fan, Martinez, G., DeSilvio, T., Shin, J., Chen, Y., Jacobs, J., Wang, B., Ozeki, T.,
 463 Lafarge, M. W., Koelzer, V. H., Barisoni, L., Madabhushi, A., Viswanath, S. E., &
 464 Janowczyk, A. (2024). CohortFinder: An open-source tool for data-driven partitioning
 465 of digital pathology and imaging cohorts to yield robust machine-learning models. *Npj
 466 Imaging*, 2(1), 15. <https://doi.org/10.1038/s44303-024-00018-2>
- 467 Fan, F., Smith, C., Nair, V., & others. (2025). Integration of pathomic signatures and spatial
 468 transcriptomics reveals tubular morphometric trajectories and enables patient stratification
 469 in minimal change disease (MCD)/FSGS: TH-OR044. *Journal of the American Society of
 470 Nephrology*, 36(10S). <https://doi.org/10.1681/ASN.2025ca1haevy>
- 471 Fogo, A. B., Lusco, M. A., Najafian, B., & Alpers, C. E. (2016). AJKD atlas of renal
 472 pathology: Ischemic acute tubular injury. *American Journal of Kidney Diseases*, 67(5), e25.
 473 <https://doi.org/10.1053/j.ajkd.2016.03.003>
- 474 Gadegbeku, C. A., Gipson, D. S., Holzman, L. B., Ojo, A. O., Song, P. X. K., Barisoni, L.,
 475 Sampson, M. G., Kopp, J. B., Lemley, K. V., Nelson, P. J., Lienczewski, C. C., Adler, S.
 476 G., Appel, G. B., Cattran, D. C., Choi, M. J., Contreras, G., Dell, K. M., Fervenza, F. C.,
 477 Gibson, K. L., ... Kretzler, M. (2013). Design of the Nephrotic Syndrome Study Network
 478 (NEPTUNE) to evaluate primary glomerular nephropathy by a multidisciplinary approach.
 479 *Kidney Int*, 83(4), 749–756. <https://doi.org/10.1038/ki.2012.428>
- 480 Gutman, D. A., Khalilia, M., Lee, S., & others. (2017). The digital slide archive: A software
 481 platform for management, integration, and analysis of histology for cancer research. *Cancer
 482 Research*, 77(21), e75–e78. <https://doi.org/10.1158/0008-5472.CAN-17-0629>
- 483 Heinrich, J., & Weiskopf, D. (2013). State of the art of parallel coordinates. In M. Sbert &
 484 L. Szirmay-Kalos (Eds.), *Eurographics 2013 - state of the art reports*. The Eurographics
 485 Association. <https://doi.org/10.2312/conf/EG2013/stars/095-116>
- 486 Image file type and format guide - Media | MDN. (2025). In *MDN Web Docs*. https://developer.mozilla.org/en-US/docs/Web/Media/Guides/Formats/Image_types
- 487 Installation — HoloViews v1.21.0. (n.d.). Retrieved July 3, 2025, from <https://holoviews.org/>
- 488 Janowczyk, A., Zuo, R., Gilmore, H., Feldman, M., & Madabhushi, A. (2019). HistoQC: An
 489 Open-Source Quality Control Tool for Digital Pathology Slides. *JCO Clin Cancer Inform*,
 490 3, CCI.18.00157. <https://doi.org/10.1200/CCI.18.00157>
- 491 Lee, D., & Seung, H. (2001). Algorithms for Non-negative Matrix Factorization. *Adv. Neural
 492 Inform. Process. Syst.*, 13.
- 493 Maaten, L. van der, & Hinton, G. (2008). Visualizing Data using t-SNE. *Journal of Machine
 494 Learning Research*, 9(86), 2579–2605. <http://jmlr.org/papers/v9/vandermaaten08a.html>
- 495 McInnes, L., Healy, J., & Melville, J. (2020). UMAP: Uniform Manifold Approximation and
 496 Projection for Dimension Reduction. arXiv. <https://doi.org/10.48550/arXiv.1802.03426>
- 497 Pallets/flask: The Python micro framework for building web applications. (n.d.). Retrieved
 498 October 28, 2025, from <https://github.com/pallets/flask/?tab=readme-ov-file>
- 499 SlickGrid Home. (n.d.). Retrieved July 9, 2025, from <https://slickgrid.net/Index.html>
- 500 TensorFlow Team. (2025). Visualizing data using the embedding projector in TensorBoard.
 501 https://www.tensorflow.org/tensorboard/tensorboard_projector_plugin.
- 502 Yun, X. (2025). BigFatDog/parcoords-es. <https://github.com/BigFatDog/parcoords-es>